Influence of hardening and inhomogenuity on internal loops in pseudoelasticity*

M.S. Kuczma† and A. Mielke

Institut für Angewandte Mathematik, Universität Hannover
Welfengarten 1, D-30167 Hannover, Germany

Version of July 21, 1998

Abstract

The paper is concerned with the mathematical modelling and computational simulation of hysteretic behaviour typically exhibited by shape memory alloys in the pseudoelastic temperature range, as observed by I. Müller and his co-workers in experimental tests for CuZnAl monocrystals. The point of departure is the one-dimensional thermomechanical model due to I. Müller and due to V.I. Levitas. The internal hysteresis loops are described by means of a discrete memory variable which can be handled by a monotone path rule. Existence and uniqueness of solutions is shown in the presence of hardening. We investigate the limit of vanishing hardening and vanishing material inhomogenuity and show that the limit depends on their relative size within the limit procedure. The analytical and numerical results show that under small hardening the phase transformation process is very sensitive to any inhomogenuities which may be present (e.g. geometric ones) or are developed in the two-phase system in the course of the loading/unloading sequences. Great differences in the local response at a material point and the system behaviour are observed, in particular the system displays internal loops only if the hardening is significantly larger than the material inhomogenuities.

1 Introduction

Pseudoelasticity is the kind of material behaviour in which, at a constant temperature, comparatively large strains as a result of loading to well above the elastic limit are completely recovered upon unloading. Pseudoelasticity has been observed in many alloys which demonstrate the shape memory effect. This phenomenon is attributed to a martensitic transformation which may, in general, be induced by either temperature or stress, [6]. Here we consider only quasistatic phase transformations which occur at a constant temperature above the austenit finish temperature. In this case there are stress-induced austenite/martensite phase

*Research supported by the VW-Stiftung within the project *Strain and stress induced phase transformations in engineering materials*, (grant I/70 284).

†On leave from the Poznan University of Technology, Piotrowo 5, PL-60965 Poznan, Poland.

transformations whose characteristic feature are stress-strain hysteresis loops in the process of subsequent loading and unloading. Our aim is a mathematical study of the qualitative behaviour of internal hysteresis loops in dependence of hardening and material homogenuity.

We use a mathematical model for the pseudoelastic behaviour that has been developed by I. Müller and his co-workers, e.g. [7] and was supplemented with a description of internal hysteresis loops by V.I. Levitas [12]. As is generally agreed, the appearence of hysteresis in solids is connected with existence of a nonconvex energy function and some microscopic energetic barriers, [4, 1, 16, 14]. In the adopted phenomenological description of the phase transformation it is assumed that two phases, here a parent phase called *austenite* ($\mathcal{A}$-phase) and a product phase called *martensite* ($\mathcal{M}$-phase) may coexist at each material point, which corresponds to the relaxation of the free energy [8]. The thermomechanical model is based on a common quadratic expression of free energy for each phase. The structural rearrangements at a micro scale are accounted for by means of an internal variable $c \in [0, 1]$ which is defined as the volume fraction (concentration) of the product phase: $c = 0$ ($c = 1$) denotes the pure $\mathcal{A}$-phase ($\mathcal{M}$-phase). The free energy of the mixture is a weighted sum of free energies of the phases and the mixing energy

$$\psi = (1 - c)\psi_{\mathcal{A}} + c\psi_{\mathcal{M}} + \psi_{\mathrm{mix}}.$$

The term we called "mixing energy" plays the fundamental role in modelling the hysteresis effects. Following the experimental evidence it is argued that the mixing energy depends on two internal variables: volume fraction c and the number of austenite-martensite interfaces, [18, 7]. However, as concerns the second internal variable the basic problem which remains open is a description of its precipitous changes in the vicinity of the phase eqilibrium line. The expression for the mixing energy which we have assumed is a quadratic function of c, with a material constant adjusted against experimental results. In Levitas [12] a phase transformation rule was derived from the second principle of thermodynamics and is based on the supposition that a phase transformation may only start if the driving force conjugate to the rate of phase fraction reaches a certain threshold value. The observed internal hysteresis loops are described by means of a memory variable c_0 which is a discontinuous function of time. As known from experiments, the $\mathcal{A} \to \mathcal{M}$ transformation is exotermic, and the reverse $\mathcal{M} \to \mathcal{A}$ transformation is endotermic. As a result, the specimen experiences self heating and cooling, which strongly influences the transformation stress. The pseudoelastic behaviour is modelled here as an isothermal quasistatic deformation-controlled process (hard loading device). The nonisothermal case will be the subject of our future work, some preliminary results are contained in [9]; see also [3, 2] and the results of comprehensive laboratory experiments of Shaw & Kyriakides [17].

After explaining the mechanical problem in more detail in Section 2. We consider a one-dimensional bar with reference configuration $x \in [0, l_B]$ which is subject to a hard loading device, that is we prescribe displacement boundary conditions $u(t, 0) = 0$ and $u(t, l_B) = \ell(t)$. Of course the model describes also plane shear experiments. In Section 3 we present several analytical results for the model. In the case with hardening we prove an existence and uniqueness result for solutions under the assumption of a piecewise monotone loading $\ell(t)$. In the case of no hardening and a homogeneous bar we show that there are infinitely many solutions displaying completely different system behaviour. Finally we investigate the limit of hardening and material inhomogenuity going to 0 simultaneously such that their relative size can be measured by a constant $\rho > 0$. In the limit we find a distinguished solution for the homogeneous problem without hardening which still depends on ρ and thus contains information about the relative size of hardening and inhomogenuity.

The analysis becomes too complicated to investigate a complete cycle with loading, unloading and reloading. Thus, we used a numerical method to calculate the system behaviour for more complex situations such as three loading cycles. Here we also use physically relevant material parameters obtained from [5]. In Section 4.1 the numerical scheme is devised by time and space discretization, and we present numerical evidence for its convergence. In Section 4.2 we then analyze the system behaviour under loading cycles.

Our findings are that in the case of large ρ (large inhomogenuity and small hardening) the system behaviour does not display internal loops since most points satisfy the condition $c = 0$ or $c = 1$ and follow the outer hysteresis loop. Only in the case of small ρ (large hardening and small inhomogenuity) the points are forced to behave similar at each point $x \in [0, l_B]$ and the system behaviour shows the desired internal loops.

This observation seems important even from the numerical point of view. Often one considers homogenous material and is interested in the behaviour of the system without hardening. However, to obtain numerical stability one introduces a small amount of hardening. Our result suggests that this hardening singles out a very particular solution which might not be the physically relevant one if material inhomogenuities (e.g. through stress concentrations or impurities) are much stronger than the hardening.

2 The mechanical model

In this section we will record the relations which define the model of ideal pseudoelasticity introduced by Müller *et al.* [7] and further discussed by Levitas [12]. Müller *et al.* carried out experimental tests on a CuZnAl single crystal specimen. The model describes the phase transformation phenomenon in the shape memory alloy at temperatures above A_f, and the adjective "ideal" refers to the idealized situation with horizontal yield and recovery lines in the stress-strain diagram. In the next section we shall assume a more general case with hardening.

Some typical pseudoelastic paths in the stress-strain diagram are shown in Fig. 1, see also [7, 12]. In the macroscopic description of a phase transformation process, a useful internal variable very often applied is a scalar c which is defined as a volume fraction of martensite in the (infinitesimal) volume of the $\mathcal{A}/\mathcal{M}$-mixture, i.e. $0 \leq c \leq 1$. In terms of the phase fraction rate $\dot{c}$ we can in general distinguish the following three characteristic stages of the deformation process, cf. Fig. 1:

1. reversible, purely elastic deformation of $\mathcal{A}$- or $\mathcal{M}$-phase or $\mathcal{A}/\mathcal{M}$-mixture: $\dot{c} = 0$;

2. direct phase transformation $\mathcal{A} \rightarrow \mathcal{M}$: $\dot{c} > 0$;

3. reverse phase transformation $\mathcal{M} \rightarrow \mathcal{A}$: $\dot{c} < 0$.

We remark that at points in the triangle ABD and line BC the rate $\dot{c}$ is positive or equal to zero, whereas at points in the traingle ADE and interval OE, $\dot{c} \leq 0$. The diagonal AD (including points A and D) plays a critical role in the process. As can be seen in Fig. 1, on the diagonal the phase transformation initiates and its direction can be reversed, depending

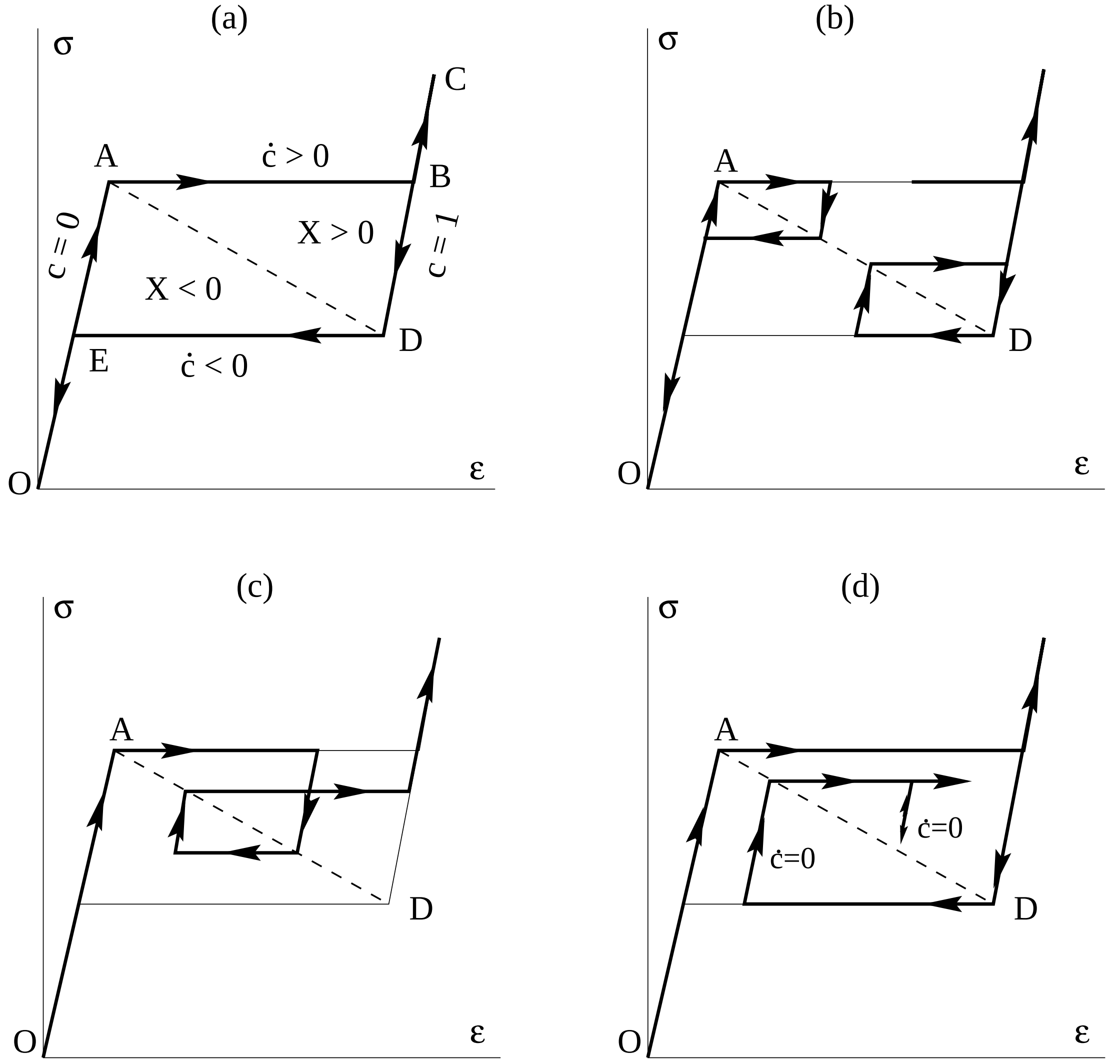

Figure 1: Stress vs strain diagram of ideal pseudoelastic behaviour. Phase transformation starts at the diagonal AD: (a) Yield and recovery; outer loop. (b) Internal yield and internal recovery. (c) Internal loop. (d) Internal elasticity and history dependence.

on the sense of strain increments. In fact, the diagonal is a phase equlibrium line but the states therein are not in a stable thermodynamic equilibrium.

We consider the simplified case that the elastic moduli in both phases are equal, i.e. $E = E_{\mathcal{A}} = E_{\mathcal{M}}$. The elastic parts of the strain are given by

$$\varepsilon^e_{\mathcal{A}} = \varepsilon, \qquad \varepsilon^e_{\mathcal{M}} = \varepsilon - \eta$$

where $\varepsilon = \partial u/\partial x$ is the derivative of displacement u, and η is the transformation strain, a positive material constant. The free energy of the mixture is the sum of contributions

$$\psi = (1-c)\psi_{\mathcal{A}}(\varepsilon^e_{\mathcal{A}}) + c\psi_{\mathcal{M}}(\varepsilon^e_{\mathcal{M}}) + \psi_{\text{mix}}(c) \tag{1}$$

in which $\psi_i = \psi_i^0(\theta) + 0.5\,E(\varepsilon_i^e)^2$ for $i \in \{\mathcal{A}, \mathcal{M}\}$ is the assumed form of the free energy for each phase that is quadratic in elastic strain. The phase-mixture energy, $\psi_{\text{mix}} = 0.5\,B(1-c)c$

was derived also in the 3D case by Levitas [13], the material constant B being related to the area of the outer hysteresis loop. In principle, the functions $\psi_i^0(\theta)$ depend on the temperature θ; however here we consider the isothermal case. Using the fact that we have $\varepsilon^e_{\mathcal{A}} = \varepsilon^e_{\mathcal{M}}$ (due to the same stresses and Young moduli in both phases) we obtain for (1) the final expression

$$\psi(\varepsilon, c) = 0.5\, E\, (\varepsilon - c\eta)^2 + (1-c)\psi^0_{\mathcal{A}} + c\psi^0_{\mathcal{M}} + 0.5\, B(1-c)c. \tag{2}$$

The second law of thermodynamics states that the rate of mechanical dissipation per unit volume, D, has to be positive. Here this implies

$$\sigma = \frac{\partial \psi}{\partial \varepsilon} = E(\varepsilon - c\eta) \tag{3}$$

and

$$D = X\dot{c} \geq 0 \quad \text{where} \quad X = -\frac{\partial \psi}{\partial c} = \sigma\eta - \Delta\psi^0 - 0.5\, B(1-2c) \tag{4}$$

is, as a variable conjugate to $\dot{c}$, the thermodynamic driving force for phase transformation and $\Delta\psi^0 = \psi^0_{\mathcal{M}} - \psi^0_{\mathcal{A}}$ is the difference in the free energies of the phases at a given temperature.

Note that the driving force is positive in the triangle ABD and negative in the triangle ADE. In order to consistently account for the experimental findings of Müller *et al.*, Levitas has used a concept of threshold value for X. According to this concept the phase transformation may take place only if the driving force X equals the threshold value, see also [15]. This idea is directly based on the dissipation inequality (4) and it postulates that

$$\text{if } X = k_{\mathcal{A}\to\mathcal{M}}(c) > 0 \quad \text{then } \dot{c} \geq 0\,, \tag{5}$$

$$\text{if } X = k_{\mathcal{M}\to\mathcal{A}}(c) < 0 \quad \text{then } \dot{c} \leq 0\,, \tag{6}$$

$$\text{if } k_{\mathcal{M}\to\mathcal{A}}(c) < X < k_{\mathcal{A}\to\mathcal{M}}(c) \quad \text{then } \dot{c} = 0. \tag{7}$$

The following situations concerning the conditions (5) and (6) deserve further comment. First, the case $X = 0$ corresponds to the states on the phase equilibrium line, the diagonal AD in Fig. 1. These states are unstable and any process along the phase equilibrium line is accompanied by no dissipation. Further, the situations $X = k_{\mathcal{A}\to\mathcal{M}}(c) > 0$ and $\dot{c} = 0$, and $X = k_{\mathcal{M}\to\mathcal{A}}(c) < 0$ and $\dot{c} = 0$ correspond to a degenerate problem in which both the complementary variables, $y^+ \equiv X - k_{\mathcal{A}\to\mathcal{M}}(c)$ and $\dot{c}$ are equal to zero, similarily for $y^- \equiv X - k_{\mathcal{M}\to\mathcal{A}}(c)$ and $\dot{c}$. That the phase transformation process, and not another one, starts on the phase equilibrium line and carry on when the condition $X = k_{\mathcal{A}\to\mathcal{M}}(c)$, or $X = k_{\mathcal{M}\to\mathcal{A}}(c)$ is satisfied, can be motivated by the principle of least work, cf. Wilmanski [19]. The threshold quantities, $k_{\mathcal{A}\to\mathcal{M}}$ for $\mathcal{A} \to \mathcal{M}$ phase transformation and $k_{\mathcal{M}\to\mathcal{A}}$ for $\mathcal{M} \to \mathcal{A}$ phase transformation are assumed here to be dependent only on the volume fraction c and a new internal variable c_0 that is equal to the value of c at the latest crossing of the diagonal AD. We adopt the functions $k_{\mathcal{A}\to\mathcal{M}}$ and $k_{\mathcal{M}\to\mathcal{A}}$ in the form

$$k_{\mathcal{A}\to\mathcal{M}} = \max\{L(c - c_0), 0\}, \qquad k_{\mathcal{M}\to\mathcal{A}} = \min\{L(c - c_0), 0\}, \tag{8}$$

The new material parameter L should be greater than or equal to B. The case $L = B$ corresponds to ideal behaviour and $L > B$ to hardening. Condition (5) is relevant for all horizontal intervals in the "upper" triangle ABD, whilst (6) controls the phase transformation process along horizontal segments in the "lower" triangle ADE. All the states on intervals parallel to lines OA and DC are governed by condition (7). These three conditions (5) – (7) when supplemented with the auxiliary one, $0 \leq c \leq 1$, allow us to describe completely the stress-strain relationship illustrated in Fig. 1, including the proper succession of states. The latter is guaranted by a suitable updating of the variable c_0. On the outer intervals, i.e. AB and DE, we take $c_0 = 0$ and $c_0 = 1$, respectively. In general, c_0 is changed at the intersection point of the actual stress-strain path and the diagonal AD (discrete memory).

It is a major goal of this work to discuss the question why the case $L = B$ (no hardening) is highly degenerate and how the limit $L \to B$ can be understood in cases where the material inhomogenuity is also small.

The mechanical problem is now completed by associating the cross-sectional area $\alpha(x)$ to each value of the axial variable $x \in [0, l_B]$, where l_B is the length of the bar. Thus, the effective elastic modulus at x is $\alpha(x)E$. The mechanical problem is now given as follows: For each $t \in [0, T]$ and each $x \in [0, l_B]$ we have

$$\boxed{\begin{gathered} \frac{\mathrm{d}}{\mathrm{d}x}\Big(\alpha(x)E[\varepsilon(t,x) - c(t,x)\eta]\Big) = 0, \\ \int_0^{l_B} \varepsilon(t,x)\,\mathrm{d}x = \ell(t), \\ (c(t,x), c_0(t,x)) \text{ satisfy the phase transformation conditions (5) — (8).} \end{gathered}} \tag{9}$$

The first equation is the elastic equilibrium equation and the second is equivalent to the displacement conditions $u(t, 0) = 0$ and $u(t, l_B) = \ell(t)$.

An important quantity in our analysis will be the axial force

$$F(t) = \alpha(x)\sigma(t,x) = \alpha(x)E(\varepsilon(t,x) - c(t,x)\eta)$$

which is constant along the bar due to the elastic equilibrium. In experiments one usually plots only the curve $(F(t), \ell(t))$ which gives the stress-strain relation. We will associate to this curve the name "*system behaviour*" as it averages over all the material points $x \in [0, l_B]$ where different local material behaviour may occur.

3 Analytical results

First, we develop a mathematical theory for the case with hardening which allows us to construct the unique solution for prescribed hard loadings $\ell(t)$ which are piecewise monotone. Here we use the special feature in the one-dimensional theory that the sign of $\dot{\ell}(t)$ determines for each point x whether there is loading or unloading. Second, we analyze the case of a homogeneous bar made of a material without hardening and show that the set of possible solutions is very rich, such that the system behaviour is not determined. Third, we consider the case $L = B + \omega$ and $\alpha(x) = \alpha_0 + \omega\rho\alpha_1(x)$ in the limit $\omega \to 0$, which provides special solutions for the homogeneous case without hardening. In particular, we discuss the differences in the unloading depending on the parameter ρ which measures the size of the inhomogenuity relative to the hardening parameter $\omega = L - B$. We find that small ρ gives rise to the internal loops presented in Fig. 3 while large ρ leads to so-called external loops.

3.1 Existence of solutions

To solve our quasistatic loading problem we have to assume that the loading function $\ell(t)$ is piecewise monotone in $[0,T]$, that is there are finitely many subintervals $[t_j, t_{j+1}]$ such that $\ell(t)$ is monotone on these subintervals. The main observation here is that in every material point the values $\sigma(t)$, $c(t)$ and $c_0(t)$ can be given as functions of $\varepsilon(t)$ and the values of $c(t_j)$ and $c_0(t_j)$ as long as $\varepsilon(\cdot)$ is monotone on $[t_j, t]$. We denote these functions as

$$\sigma(t) = \Sigma(\varepsilon(t), c(t_j), c_0(t_j)),\ \ c(t) = \mathcal{C}(\varepsilon(t), c(t_j), c_0(t_j)),\ \ c_0(t) = \mathcal{C}_0(\varepsilon(t), c(t_j), c_0(t_j)). \quad (10)$$

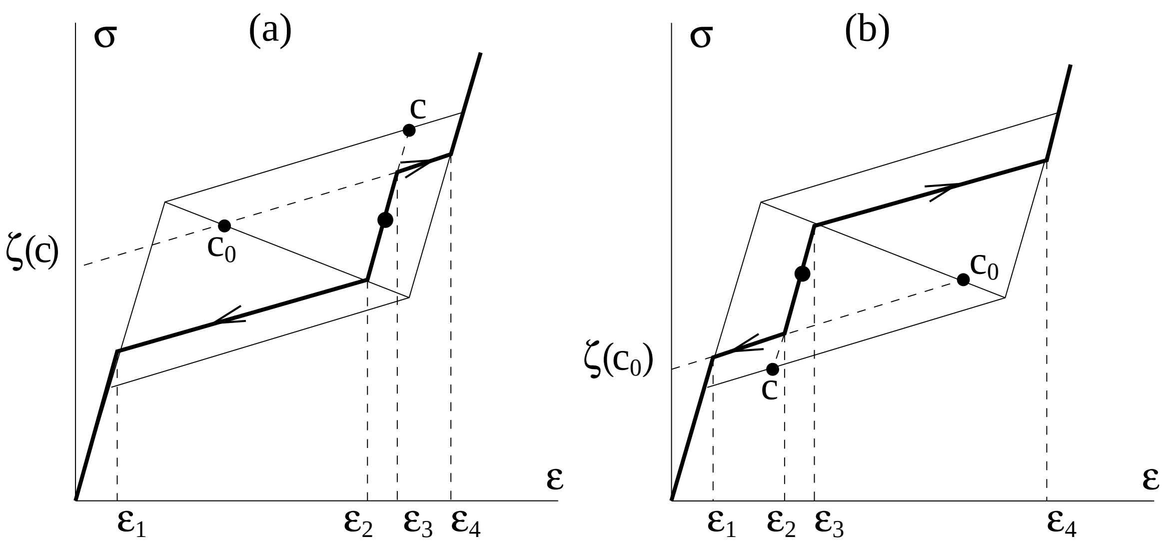

Figure 2: Illustration for determining the function Σ: (a) Case $c > c_0$, (b) Case $c < c_0$.

Some elementary calculations using the phase transformation rules give the following explicit expressions.

$$\Sigma(\varepsilon, c, c_0) = \begin{cases} E\varepsilon & \text{for } \varepsilon \leq \varepsilon_1(c, c_0), \\ \tilde{E}\varepsilon + E\eta\xi(\max\{c, c_0\}) & \text{for } \varepsilon_1(c, c_0) \leq \varepsilon \leq \varepsilon_2(c, c_0), \\ E\varepsilon - \mu c & \text{for } \varepsilon_2(c, c_0) \leq \varepsilon \leq \varepsilon_3(c, c_0), \\ \tilde{E}\varepsilon + E\eta\xi(\min\{c, c_0\}) & \text{for } \varepsilon_3(c, c_0) \leq \varepsilon \leq \varepsilon_4(c, c_0), \\ E\varepsilon - \mu & \text{for } \varepsilon_4(c, c_0) \leq \varepsilon, \end{cases} \quad (11)$$

wherein the characteristic strains, ε_i, and ξ are given by

$$\begin{aligned} \varepsilon_1(c, c_0) &= (\gamma - L\max\{c, c_0\})/\mu, \\ \varepsilon_2(c, c_0) &= (\gamma + \nu c - L\max\{c, c_0\})/\mu, \\ \varepsilon_3(c, c_0) &= (\gamma + \nu c - L\min\{c, c_0\})/\mu, \\ \varepsilon_4(c, c_0) &= (\gamma + \nu - L\min\{c, c_0\})/\mu, \\ \xi(\tilde{c}) &= (\gamma - L\tilde{c})/\nu, \end{aligned} \quad (12)$$

with the material parameters $\mu = E\eta$, $\tilde{E} = (L-B)E/\nu$, $\nu = L-B+E\eta^2$ and $\gamma = B/2+\Delta\psi^0$.

Moreover, we obtain

$$\mathcal{C}(\varepsilon, c, c_0) = \begin{cases} 0 & \text{for } \qquad\qquad \varepsilon \le \varepsilon_1(c, c_0), \\ \mu\varepsilon/\nu - \xi(\max\{c, c_0\}) & \text{for } \varepsilon_1(c, c_0) \le \varepsilon \le \varepsilon_2(c, c_0), \\ c & \text{for } \varepsilon_2(c, c_0) \le \varepsilon \le \varepsilon_3(c, c_0), \\ \mu\varepsilon/\nu - \xi(\min\{c, c_0\}) & \text{for } \varepsilon_3(c, c_0) \le \varepsilon \le \varepsilon_4(c, c_0), \\ 1 & \text{for } \varepsilon_4(c, c_0) \le \varepsilon, \end{cases} \tag{13}$$

$$\mathcal{C}_0(\varepsilon, c, c_0) = \begin{cases} c_0 & \text{if } (\varepsilon > \varepsilon_2(c, c_0) \text{ and } c > c_0) \text{ or if } (\varepsilon < \varepsilon_3(c, c_0) \text{ and } c < c_0), \\ c & \text{if } (\varepsilon \le \varepsilon_2(c, c_0) \text{ and } c > c_0) \text{ or if } (\varepsilon \ge \varepsilon_3(c, c_0) \text{ and } c < c_0). \end{cases} \tag{14}$$

With these three functions we are now able to construct a solution of our problem (9).

Theorem 1 *Assume $L > B$ and let $\ell : [0, T] \to \mathbf{R}$ be a continuous, piecewise monotone function. Then, problem (9) has a unique solution which is also piecewise monotone in ε on the same time intervals.*

Proof. Let $0 = t_0 < t_1 < \ldots < t_{n-1} < t_n = T$ be the partition of $[0, T]$ such that $\ell(\cdot)$ is monotone on $[t_j, t_{j+1}]$. Assume the solutions are calculated up to $t = t_j$. We now construct the solution such that $\varepsilon(\cdot, x)$ has the same monotonicity as ℓ on $[t_j, t_{j+1}]$. Using the elastic equilibrium in (9) we find

$$\alpha(x)\Sigma(\varepsilon(t, x), c(t_j, x), c_0(t_j, x)) = F(t) \text{ for } x \in [0, l_B].$$

where $F(t)$ is the undetermined axial force. Since $\sigma = \Sigma(\varepsilon, c, c_0)$ can be inverted in the form $\varepsilon = \mathcal{E}(\sigma, c, c_0)$, the axial force can be found from the length condition

$$\ell(t) = \mathcal{L}(F(t), t_j) \stackrel{\text{def}}{=} \int_0^{l_B} \mathcal{E}(\frac{F(t)}{\alpha(x)}, c(t_j, x), c_0(t_j, x))\, \mathrm{d}x.$$

Since Σ is piecewise linear in ε with derivatives $E, \tilde{E} > 0$ it is easy to see that $\mathcal{L}(F, t_j)$ is monotone in F with a slope between $1/E$ and $1/\tilde{E}$. Thus, $F(t)$ is uniquely determined from $\ell(t)$ and has the same monotonicity. Now for $t \in [t_j, t_{j+1}]$ the desired solution is given by $\varepsilon(t, x) = \mathcal{E}(\frac{F(t)}{\alpha(x)}, c(t_j, x), c_0(t_j, x))$, $c(t, x) = \mathcal{C}(\varepsilon(t, x), c(t_j, x), c_0(t_j, x))$ and $c_0(t, x) = \mathcal{C}_0(\varepsilon(t, x), c(t_j, x), c_0(t_j, x))$. This proves the result. QED

We believe that uniqueness in the class of all solutions holds, not just in the class of monotone solutions. However, we were unable to show this.

3.2 The homogeneous case without hardening

The above method certainly does not work in the case $L = B$ since this implies $\tilde{E} = 0$. We now show that this case leads to a big variety of solutions if additionally $\alpha(x) \equiv \alpha_0$, that is the bar is homogeneous. To illustrate the fact we consider a simple loading and unloading cycle $\ell(t) = \ell_{\max}(1 - |1 - t|)$ which however only reaches the maximal value $\ell_{\max} = l_B(\gamma/\mu + \eta/2)$ which is half way in the hysteresis loop. Starting with $c(0, x) = c_0(0, x) = 0$ we obtain for

$\ell(t) \leq l_B\gamma/\mu$ that $c(t,x)$ and $c_0(t,x)$ remain 0 since we are below the critical strain. However, for $\ell(t) > l_B\gamma/\mu$ and $t < 1$ the only constraints on $c(t,x)$ are

$$\frac{\partial}{\partial t}c(t,x) \geq 0, \quad \int_0^{l_B} \left(\frac{\gamma}{\mu} + c(t,x)\eta\right) \mathrm{d}x = \ell(t).$$

Clearly there are a lot of ways to satisfy these conditions. For instance we may take $c(t,x) = (\mu\ell(t) - l_B\gamma)/(\mu\eta l_B)$ or we choose $c(t,x) = 1$ for $x \in [x_1(t), x_2(t)]$ and 0 otherwise, where $\dot{x}_1(t) \leq 0$ and $\dot{x}_2(t) \geq 0$ with $x_2(t) - x_1(t) = (\mu\ell(t) - l_B\gamma)/(\mu\eta)$. The function $c_0(t,x)$ remains 0 for all $t \in [0,1]$.

In this loading process we still have the same axial force $F(t)$ for all the different solutions, namely $F(t) = \alpha_0 E \min\{\gamma/\mu, \ell(t)/l_B\}$, so the system behaviour does not reflect the nonuniqueness. This will be completely different upon unloading. As a result of the loading process we obtain a general function $c(1,x) \in [0,1]$ with the only side condition $\int_0^{l_B} c(1,x)\,\mathrm{d}x = l_B/2$. For simplicity we may assume that $c(1,\cdot)$ attains the n values $0 < c_1 < c_2 < \ldots < c_n \leq 1$ in intervals of the length $\delta_j l_B$, $j = 1,\ldots,n$; then $\int_0^{l_B} c(1,x)\,\mathrm{d}x = l_B \sum_1^n \delta_j c_j = l_B/2$. Upon unloading the axial force decreases and the points in intervals with $2Bc_j < \gamma - \mu F(t)/(\alpha_0 E)$ have passed the diagonal and are thus transformed back completely into $c(2,x) = 0$ with $c_0(2,x) = c(1,x)$. Hence, the unloading path is piecewise linear and consist of purely elastic unloadings interrupted by flat parts where successively the intervals with $c(1,x) = c_j$ are transformed back. We clearly see that there is a big freedom in choosing such unloading paths, since the height of the elastic unloading pieces is $\alpha_0 EB\delta_j c_j/\mu$ while the length of the flat parts is $\eta\delta_j(c_j - c_{j+1})$. Moreover if we consider $n \to \infty$, a general continuous $c(1,x)$ together with its unloading paths can be approximated.

We illustrate the effects of nonuniqueness more precisely by considering the system behaviour under the sequence of loading, unloading and reloading for two extreme situations: Case 1, the homogeneous state, $c(t,x) \equiv c(t)$, and Case 2, the c-inhomogeneous case of $c(t,x) \in \{0,1\}$. To this end we extend the loading program $\ell(t)$ by adding a reloading step, i.e. $\ell(t) = \ell_{\max}\max\{1 - |1-t|, t - 2/3\}$.

Case 1: For the homogeneous distribution of c we have the following evolution of force F_1,

$$F_1(t) = \begin{cases} \alpha_0 E \min\{\ell(t)/l_B, \gamma/\mu\} & \text{for } t \in [0,1], \quad \text{(loading)} \\ \alpha_0 E \max\{\ell(t)/l_B - \eta/2, \gamma/\mu - B/(2\mu)\} & \text{for } t \in [1,4/3], \quad \text{(unloading)} \\ \alpha_0 E \min\{\ell(t)/l_B - A_0, A_1\} & \text{for } t \in [4/3,2], \quad \text{(reloading)} \end{cases}$$

where $A_0 = \eta/3 - \gamma/(3\mu) + B/(2\mu)$, $A_1 = (4\gamma + 2\nu + B + B(2\gamma - 3B)/\nu)/(6\mu)$.

Case 2: We consider the case that $c(t,x) = 1$ for $x \leq x_f(t)$ and $c(t,x) = 0$ else. Hence, only the position of $x_f(t)$ has to be determined. Using the phase transformation rules we easily obtain

$$F_2(t) = \begin{cases} \alpha_0 E \min\{\ell(t)/l_B, \gamma/\mu\} & \text{for } t \in [0,1], \quad \text{(loading)} \\ \alpha_0 E \max\{\ell(t)/l_B - \eta/2, (\gamma - B)/\mu\} & \text{for } t \in [1,4/3], \quad \text{(unloading)} \\ \alpha_0 E \min\{\ell(t)/l_B - A_2, \gamma/\mu\} & \text{for } t \in [4/3,2], \quad \text{(reloading)} \end{cases}$$

where $A_2 = (3B + \eta\mu - \gamma)/(3\mu)$.

Both hysteresis loops are depicted in Fig. 3.

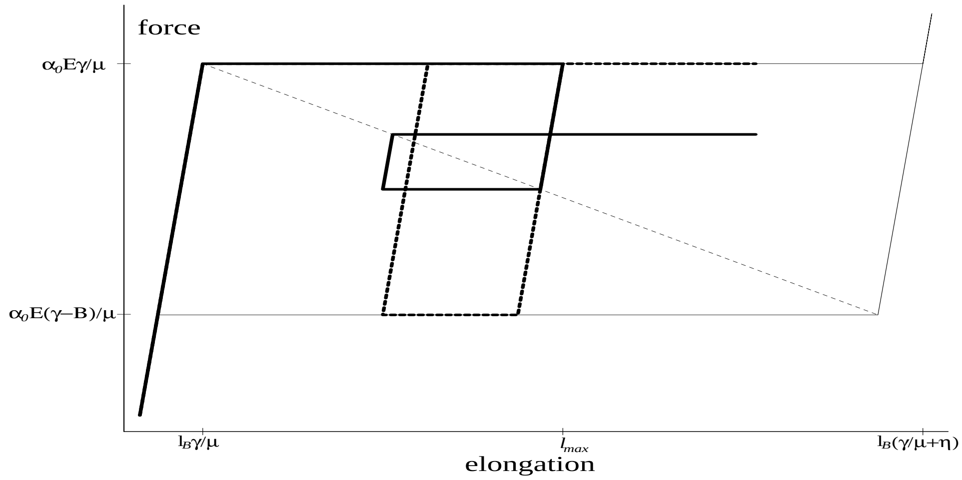

Figure 3: Nonunique system behaviour of a homogeneuous bar: (i) for homogeneuous distribution of $c(t) \in [0,1]$ (solid bold line), (ii) for inhomogeneuous distribution of c, $c(t,x) \in \{0,1\}$ (dotted bold line).

3.3 Small hardening versus small inhomogenuity

We now study the physically interesting case that the hardening parameter $L-B$ as well as the inhomogenuity of the bar, $\alpha'(x)$ are small. To this end consider the following ansatz

$$L = B + \omega\,, \qquad \alpha(x) = \alpha_0 + \omega\rho\alpha_1(x).$$

According to Subsection 3.1 there is for each piecewise monotone loading curve $\ell(t)$ a unique solution $(\varepsilon_{\omega,\rho}(t,x), c_{\omega,\rho}(t,x), c_{0,\omega,\rho}(t,x))$, and it is our aim in this subsection to show that for $\omega \to 0$ these solutions converge to a well-defined limit $(\varepsilon_{*,\rho}(t,x), c_{*,\rho}(t,x), c_{0,*,\rho}(t,x))$. This limit is in fact one of the solutions for the homogeneous problem without hardening considered in Subsection 3.2. However, it is the specific solution which still has information on the relative size of the inhomogenuity and the hardening which is expressed in the parameter ρ.

To avoid the complicated notations and to concentrate on the essentials we now choose a special set of parameters that makes the calculations simple. However, the analysis is exactly the same as for a general situation. We let

$$E = 1,\ l_B = 1,\ \eta = 4,\ B = 1,\ \gamma = 8,\ L = 1 + \omega,\ \alpha(x) = 1 + \omega\rho x.$$

This implies $\mu = 4$, $\nu = 16 + \omega$ and $\tilde{E} = \omega/(16+\omega)$. The (ε, σ) coordinates of the four points of the hystersis loop are given by

$$((7-\omega)/4, (7-\omega)/4),\ (2,2),\ (23/4, 7/4) \text{ and } ((24+\omega)/4, 2+\omega/4).$$

Moreover, we consider the representative loading $\ell(t) = 4 - |4-t|$.

We start with $c(0,x)=c_0(0,x)=0$ and find that until $t=2$ no phase transformation occurs. For solving

$$\alpha(x)\Sigma(\varepsilon(t,x),0,0)=F(t),\qquad \int_0^1 \varepsilon(t,x)\,\mathrm{d}x=\ell(t)$$

for $t\in(2,4]$ we note that the bar will generally consist of three parts, which are separated by the points $0\le x_1(t)<x_2(t)\le 1$. On $[0,x_1(t)]$ we have $c\equiv 1$ and on $[x_2(t),1]$ we have $c\equiv 0$ while in the middle there is a phase mixture.

On these three intervals we have $\varepsilon=\mathcal{E}(F/\alpha,0,0)$ explicitly and obtain the relations

$$\begin{aligned}&F/\alpha(x_1)=2+\omega/4,\quad F/\alpha(x_2)=2,\\ &\int_0^{x_1}(\frac{F}{\alpha(x)}+4)\,\mathrm{d}x+\int_{x_1}^{x_2}\frac{(16+\omega)F/\alpha(x)-32}{\omega}\,\mathrm{d}x+\int_{x_2}^{1}\frac{F}{\alpha(x)}\,\mathrm{d}x=\ell(t).\end{aligned}$$

Expanding $F=2+\omega f+\mathcal{O}(\omega^2)$ and $x_j=y_j+\mathcal{O}(\omega)$ we find, after equating the lowest order terms, the three equations

$$2\rho y_1-f=-1/4,\quad 2\rho y_2-f=0,\quad 4\rho(y_1^2-y_2^2)+(1-4f)y_1+4fy_2=(\ell(t)-2)/4.\quad (15)$$

This system has the unique solution $f=(\ell-2)\rho/2+1/8$, $y_1=(\ell-2)/4-1/(16\rho)$ and $y_2=(\ell-2)/4+1/(16\rho)$. However, this is only relevant as long as $0<y_1<y_2<1$. Whenever one or both of the values y_j do not satisfy the bound we have to set it equal to $y_j=j-1$ and omit the corresponding equation in (15). For the triple (y_1,y_2,f) we arrive at,

$$(y_1(t),y_2(t),f(t))=$$

$$\begin{cases}\Big(0,\sqrt{(\ell(t)-2)/(16\rho)},\sqrt{(\ell(t)-2)\rho/4}\Big) & \text{for } \ell(t)\in[2,2+\xi(\rho)],\\ \begin{array}{ll}(0,1,\dfrac{\ell(t)-2}{16}+\rho) & \text{if } \rho\le\rho_0\\ (\dfrac{4\rho(\ell(t)-2)-1}{16\rho},\dfrac{4\rho(\ell(t)-2)+1}{16\rho},\dfrac{4\rho(\ell(t)-2)+1}{8}) & \text{if } \rho\ge\rho_0\end{array} & \text{for } \ell(t)\in[2+\xi(\rho),6-\xi(\rho)],\\ (1-\sqrt{(6-\ell(t))/(16\rho)},1,1/4-\sqrt{(6-\ell(t))\rho/4}+2\rho) & \text{for } \ell(t)\in[6-\xi(\rho),6],\end{cases}$$

wherein $\xi(\rho)=1/(4\rho)$ if $\rho\ge\rho_0$ and $\xi(\rho)=16\rho$ if $\rho\le\rho_0$ with $\rho_0=\alpha_0/(\gamma l_B)=1/8$.

This allows us to expand also the functions $\varepsilon(t,x)$ and $c(t,x)=\hat{c}(t,x)+\mathcal{O}(\omega)$. We only give $\hat{c}(4,x)$ since it is needed for the unloading:

$$\hat{c}(4,x)=\begin{cases}1 & \text{for } x\le(8\rho-1)/(16\rho),\\ 1/2+4\rho(1-2x) & \text{for } x\in[(8\rho-1)/(16\rho),(8\rho+1)/(16\rho)],\\ 0 & \text{for } x\ge(8\rho+1)/(16\rho).\end{cases}$$

Clearly, the function c_0 is still identically 0.

In the limit $\omega\to 0$ the system behaviour is given by

$$(F_*(t),\ell(t))=(\min\{t,2\},t)\quad \text{for } t\in[0,4].$$

Thus, in the loading process we do not see any dependence on the parameter ρ. Yet, this will change dramatically in the unloading, which is sensitive to the function $c(4,x)$.

We now analyze the unloading with $\ell(t) = 8 - t$ for $t \in [4,8]$. As above the bar can be partitioned into four intervals by the boundaries $0 \le x_1 < x_2 < x_3 \le 1$, where x_1 is as before. The point $x_2(t)$ is characterized by the fact that (ε, σ) lies on the diagonal; and $x_3(t)$ is the first point where $c(t,x) = 0$. This gives the relations

$$4\frac{F(t)}{\alpha(x_2(t))} + c(4, x_2(t)) = 8, \quad 4\frac{F(t)}{\alpha(x_3(t))} + (1+\omega)c(4, x_3(t)) = 8. \tag{16}$$

The latter relation arises from the condition $F/\alpha = \sigma = E\varepsilon$ with $E = 1$ and from $\varepsilon = \varepsilon_1(c, c_0) = 2 - (1+\omega)c/4$ with $(c, c_0) = (c(4, x_3(t)), 0)$.

The point x_1 can only be moved by merging with x_2, thus it stays fixed to the value $x_1(4)$ as long as $x_2 > x_1(4)$. After that we have $x_1(t) = x_2(t)$. Note that (16) implies $x_3 - x_2 = \mathcal{O}(\omega)$; hence expanding in terms of ω we find, by equating terms of order ω^0 the conditions

$$4F_* + \hat{c}(4, y_2) = 8, \; 4F_* + \hat{c}(4, y_3) = 8, \; 4y_1 + F_* + (\hat{c}(4, y_1)^2 - \hat{c}(4, y_2)^2)/(4\rho) = \ell(t). \tag{17}$$

Here $F(t) = F_*(t) + \mathcal{O}(\omega)$. The third equation is the length condition where we have used $\int_{y_1}^{y_2} \hat{c}(4,z)\,\mathrm{d}z = (\hat{c}(4,y_1)^2 - \hat{c}(4,y_2)^2)/(16\rho)$.

For $\rho > 1/8$ we find three regimes: (i) for $\ell \in ((15\rho - 1)/(4\rho), 4]$ we have $0 < y_1 < y_2 < 1$, (ii) for $\ell \in (7/4, (15\rho-1)/(4\rho)]$ we have $0 < y_1 = y_2 < 1$ and (iii) for $\ell \le 7/4$ we have $0 = y_1 = y_2$. This produces the following system behaviour which strongly depends on ρ:

For $t \in [4,8]$ and $\rho \ge 1/8$ we have $\ell(t) = 8 - t$

$$F_*(t) = \begin{cases} 2 + \frac{\rho}{8} - \frac{1}{4}\sqrt{(\rho/2)^2 + 4\rho(t-4)} & \text{for } t \in [4, 17/4 + 1/(4\rho)], \\ 7/4 & \text{for } t \in [17/4 + 1/(4\rho), 25/4], \\ 8 - t & \text{for } t \ge 25/4. \end{cases}$$

Similarly, we can analyze the case $\rho < 1/8$ by taking into account that $\hat{c}(4,x)$ lies strictly between 0 and 1, hence $x_1 = 0$ and $x_2 = x_3 = 1$ as long as $4F(t)/\alpha(1) + c(4,1) \ge 8$. A discussion as above yields

For $t \in [4,8]$ and $\rho \le 1/8$ we have $\ell(t) = 8 - t$

$$F_*(t) = \begin{cases} 6 - t & \text{for } t \in [4, 33/8 - \rho], \\ 2 + \frac{\rho}{8} - \frac{1}{4}\sqrt{(\rho/2)^2 + 4\rho(t-6) + (1/2 + 4\rho)^2} & \text{for } t \in [33/8 - \rho, 49/8 + \rho], \\ 8 - t & \text{for } t \ge 49/8 + \rho. \end{cases}$$

It is interesting to note that the curve $(F_*(t), \ell(t))$ does not behave monotonously in ρ, see Fig. 4.

In both cases the functions $c(t,x)$ and $c_0(t,x)$ satisfy

$$c(t,x) = \begin{cases} c(4,x) & \text{for } x \le x_2(t), \\ 0 & \text{for } x \ge x_3(t); \end{cases} \qquad c_0(t,x) = \begin{cases} 0 & \text{for } x \le x_2(t), \\ c(4,x) & \text{for } x \ge x_2(t). \end{cases}$$

For $t \in [25/4, 8]$ we thus have $c(t,x) = 0$ and $c_0(t,x) = c(4,x) = \hat{c}(4,x) + \mathcal{O}(\omega)$.

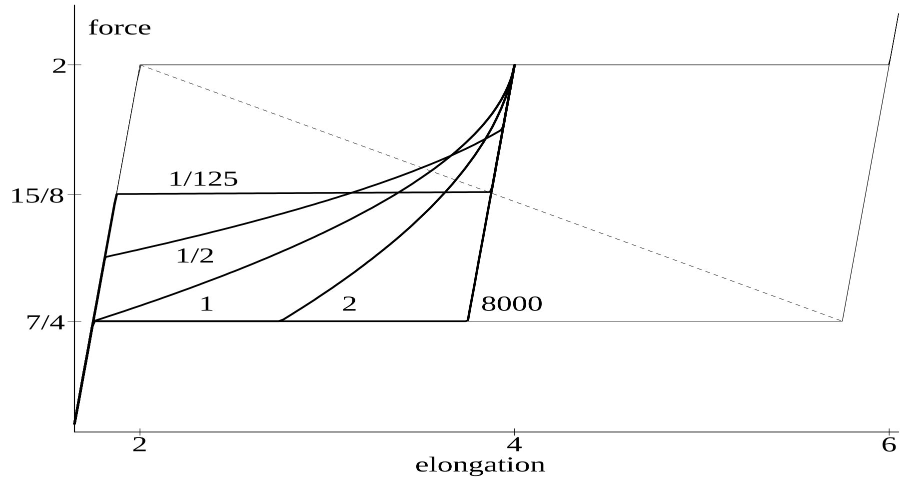

Figure 4: Force F during unloading as the function of elongation $\ell(t) = 8 - t,\ t \in [4, 8]$, for various (scaled) inhomogenuity parameters ρ/ρ_0.

We especially recall the two extreme cases of (i) hardening without inhomogenuity ($\rho \to 0$) and (ii) of large inhomogenuity and small hardening ($\rho \to \infty$). In both cases we have two purely elastic regions close to $\ell = 0$ and $\ell = 4$. In between there is a flat part of the curve which has the level 15/8 in case (i) and the level 7/4 in case (ii), see Fig. 4. Thus, the case (ii) yields weaker system behaviour.

In principle, it would be possible to analyze more complex loading cycles mathematically. However, this will lead to lengthy formulae which are difficult to discuss. Instead we will demonstrate the system behaviour in the more complex case using a numerical algorithm.

4 Numerical results

In Section 4.1 we present an iterative algorithm for solving (18) and we test its convergence numerically. The analyzed problem is a tensile test on a pseudoelastic bar with nonlinearly variable cross section and simultaneously subjected to a body force. In Section 4.2 we then present the final study of the dependence of internal hystersis loops on the relative size of hardening and inhomogenuity.

4.1 A numerical algorithm

We now consider a slightly more general problem in allowing for a volume forcing $f(t, x)$ along the bar, that is the elastic equilibrium equation is replaced by

$$\frac{\mathrm{d}}{\mathrm{d}x}\left(\alpha(x)E(\varepsilon(t,x) - c(t,x)\eta)\right) = f(t,x) \quad \text{for } x \in [0, l_B].$$

The reason for this generalization is that in this situation the monotonicity argument employed in the case $f(t, x) \equiv 0$ is no longer valued. We may have loading and unloading at the same time instant but at different material points. The ability to handle such circumstances is necessary when considering higher-dimensional problems, since then one cannot guarantee simultaneous loading or unloading even when no volume forces are present, [11].

We discretize the problem in time by selecting on the time interval $[0, T]$ nodal points t_τ, $\tau = 0, 1, ..., \bar{N}$, so a typical time-step $t_\tau \Longrightarrow t_{\tau+1}$ is defined on the time increment $\vartheta_\tau = t_{\tau+1} - t_\tau$. In the implicit time integration scheme we determine the state of the process

$$S_{\tau+1} \equiv (u_{\tau+1}, c_{\tau+1}, c_{0,\tau+1})$$

at time level $t_{\tau+1}$ for the given values of driving quantities $l_{\tau+1} = \ell(t_{\tau+1})$ and $f_{\tau+1} = f(t_{\tau+1}, \cdot)$ at this moment, and previously state S_τ.

Notice that the phase transformation problem under consideration falls into the class of free boundary problems since the boundary between the elastic region in which $c = 0$ or $c = 1$ and the phase transformation region in which $c \in (0, 1)$ is not known a priori. In addition, although this problem is explicitly defined on the field of displacement u and that of phase fraction c, actually, it also depends on the discrete-memory variable c_0. Due to the history dependence of the phase transition process we cannot determine the state $S_{\tau+1}(x)$ without knowing the path in the stress-strain diagram the material point $x \in \Omega$ has chosen, compare Fig. 5. For this reason we restrict the path in **one** time step to be as simple as possible which leads to the monotone path rule.

Monotone path rule for time steps (MPR)

In each time-step $t_\tau \Longrightarrow t_{\tau+1}$ the deformation process in a material point x is either pure loading [$\dot{\varepsilon} > 0$ $(\dot{\sigma} \geq 0)$] or pure unloading [$\dot{\varepsilon} < 0$ $(\dot{\sigma} \leq 0)$].

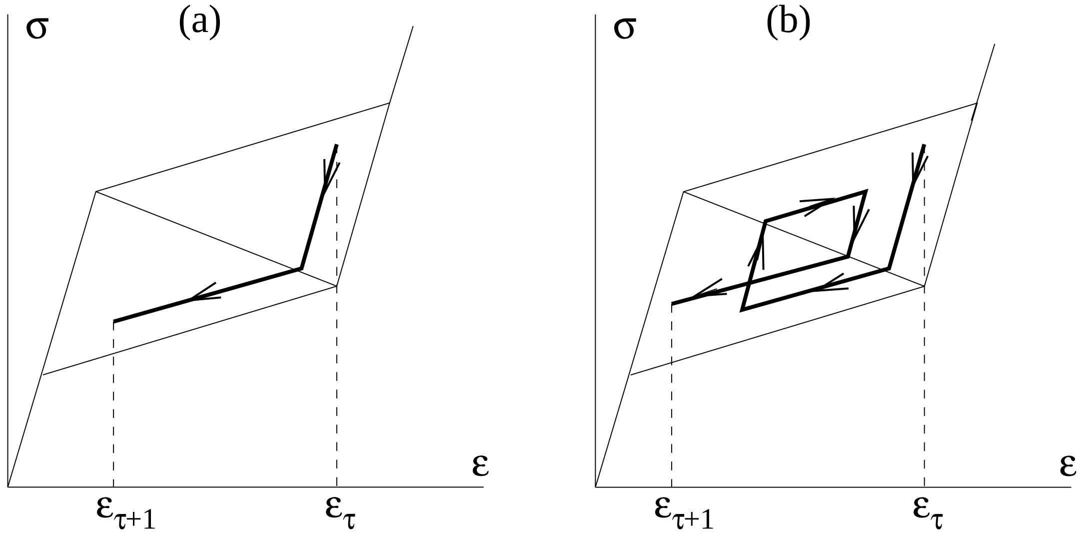

Figure 5: (a) An allowed path and, (b) an excluded path in one time-step.

Thus, according to the MPR we admit to the paths as shown, for example, in Fig. 5a, but exclude loops around the diagonal $X = 0$ as illustrated in Fig. 5b, within one time-step, at the material point at a fixed temperature. Of course, in different material points x we may have loading or unloading. An immediate consequence of MPR is that we have knowledge of the process by controlling either σ or ε alone, at a material point. This means that on a monotone path σ, c and c_0 can be written as functions of ε and the old values of $c_\tau, c_{0,\tau}$ with the function Σ, $\mathcal{C}$ and $\mathcal{C}_0$ defined in Section 3:

$$\sigma_{\tau+1} = \Sigma(\varepsilon_{\tau+1}, c_\tau, c_{0,\tau}),\ \ c_{\tau+1} = \mathcal{C}(\varepsilon_{\tau+1}, c_\tau, c_{0,\tau}),\ \ c_{0,\tau+1} = \mathcal{C}_0(\varepsilon_{\tau+1}, c_\tau, c_{0,\tau}).$$

The hysteretic evolution of the binary alloy can now be approximated by the following time-incremental problem

Given $S_\tau = (u_\tau, c_\tau, c_{0,\tau})$ find $S_{\tau+1} = (u_{\tau+1}, c_{\tau+1}, c_{0,\tau+1})$ from $u_{\tau+1}(x) = \int_0^x \varepsilon_{\tau+1}(y)\,\mathrm{d}y$ and the following relations:

$$\begin{gathered} \alpha(x)\,\Sigma\left(\varepsilon_{\tau+1}(x), c_\tau(x), c_{0,\tau}(x)\right) = F_{\tau+1} - \int_x^{l_B} f_{\tau+1}(y)\,\mathrm{d}y \text{ for } x \in [0, l_B], \\ \int_0^{l_B} \varepsilon_{\tau+1}(x)\,\mathrm{d}x = l_{\tau+1}, \\ c_{\tau+1}(x) = \mathcal{C}(\varepsilon_{\tau+1}(x), c_\tau(x), c_{0,\tau}(x)), \quad c_{0,\tau+1}(x) = \mathcal{C}_0(\varepsilon_{\tau+1}(x), c_\tau(x), c_{0,\tau}(x)). \end{gathered} \tag{18}$$

For $L > B$ we obtain a unique solution of the incremental problem by determining the unknown axial force $F_{\tau+1}$ such that the length condition holds. Moreover, the components $u_{\tau+1}$ and $c_{\tau+1}$ of $S_{\tau+1}$ depend Lipschitz continuously on the data. More precisely, there is a constant $C > 0$ such that for two different sets of data $(l^{(j)}, f^{(j)}, c^{(j)}, c_0^{(j)}) \in I\!R \times H^{-1}(\Omega) \times (L^\infty(\Omega))^2$ the solutions $S^{(j)} = (\tilde{u}^{(j)}, \tilde{c}^{(j)}, \tilde{c}_0^{(j)})$ of (18) satisfy

$$\begin{aligned} &\|\tilde{u}^{(1)} - \tilde{u}^{(2)}\|_{W^{1,\infty}(\Omega)} + \|\tilde{c}^{(1)} - \tilde{c}^{(2)}\|_{L^\infty(\Omega)} \\ &\leq C\left(|l^{(1)} - l^{(2)}| + \|f^{(1)} - f^{(2)}\|_{H^{-1}(\Omega)} + \|c^{(1)} - c^{(2)}\|_{L^\infty(\Omega)} + \|c_0^{(1)} - c_0^{(2)}\|_{L^\infty(\Omega)}\right). \end{aligned} \tag{19}$$

The existence and uniqueness follows from the fact that Σ is strictly monotone in ε, namely piecewise linear with slopes either $E > 0$ or $\tilde{E} > 0$. The comparison estimate follows by using the Lipschitz continuity of Σ and $\mathcal{C}$ in their arguments. A similar estimate for c_0 does not hold since $\mathcal{C}_0$ has jumps. Whenever a loading path slightly crosses the diagonal and then the direction of the response is reversed we have unstable behaviour: compare the paths for a single material point in Figs. 6a and 6b, where the deformation process depends discountinuously on the loading history.

The discontinuity shows that it is not possible to use standard methods to prove convergence of the incremental method proposed above, since the initial-value problem is not well-posed. Nevertheless in practical situations one observes numerical convergence. This might be due to the fact that the critical points which show discontinuous dependence on the initial data are usually on a set of very small measure.

The first two equations in (18) have to be solved numerically. This can be done as follows. The function $\mathcal{E}(\sigma, c, c_0)$ as the inverse of $\sigma = \Sigma(\varepsilon, c, c_0)$ is known explicitly, compare the proof

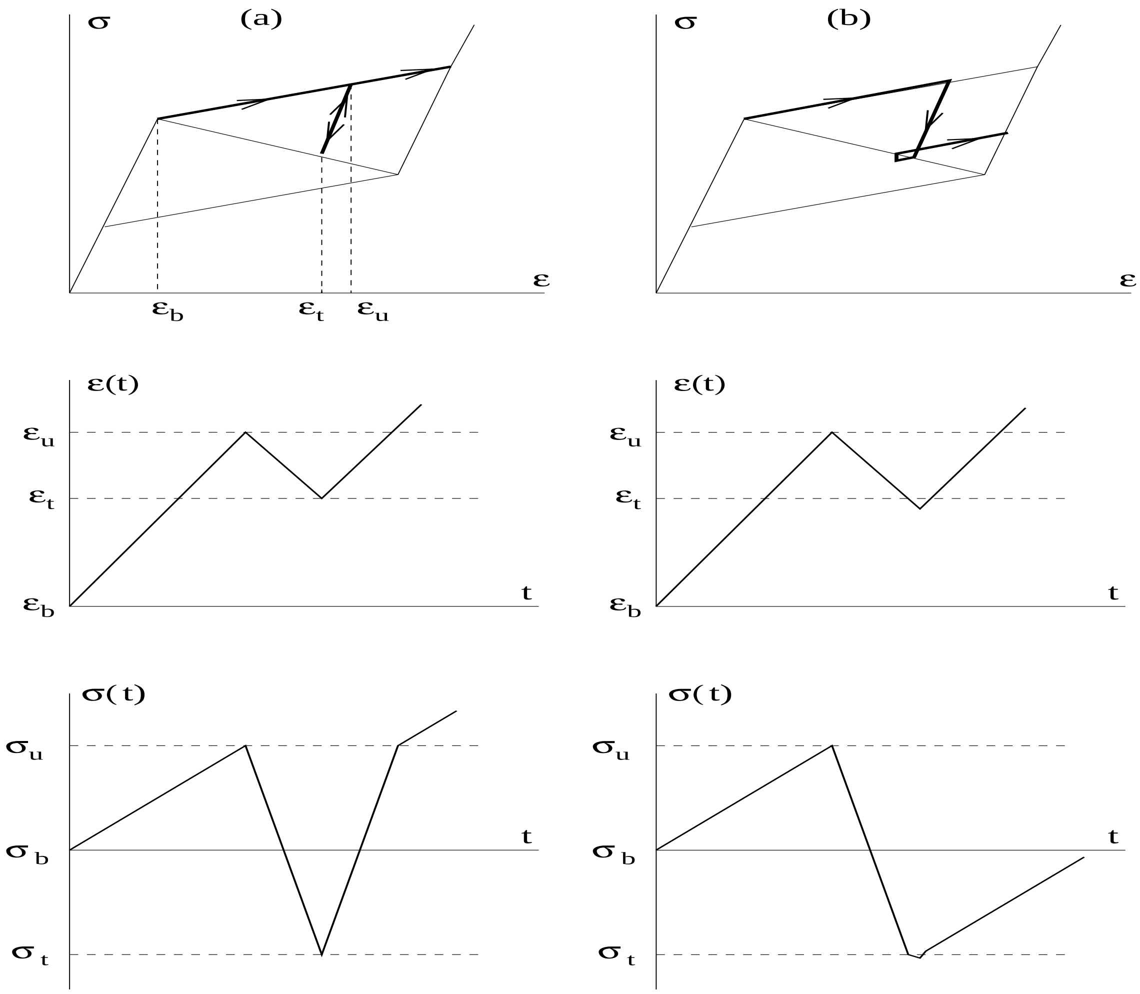

Figure 6: Illustration of a discontinuous response of the thermomechanical model.

in Section 3.1. Hence it remains to solve

$$\begin{aligned} l_{\tau+1} &= \mathcal{L}_{\tau+1}(F_{\tau+1}) \stackrel{\text{def}}{=} \int_0^{l_B} \mathcal{E}(\sigma(x), c_\tau(x), c_{0,\tau}(x))\,\mathrm{d}x \\ \text{with} \qquad & \sigma(x) = (F_{\tau+1} - \int_x^{l_B} f_{\tau+1}(y)\,\mathrm{d}y)/\alpha(x). \end{aligned} \tag{20}$$

To solve this nonlinear scalar problem we introduce a node spacing $x_i = ih$, $i = 0, 1, 2, \ldots, M$, with $h = l_b/M$. The integrals are then calculated by a trapeziodal rule and the nonlinear scalar function is solved using bisection with a relative error in $l_{\tau+1}$ smaller than 10^{-12}. Then $\varepsilon_{\tau+1}$, $c_{\tau+1}$ and $c_{0,\tau+1}$ are obtained on the nodes x_i via $\mathcal{E}$, $\mathcal{C}$ and $\mathcal{C}_0$ as explained above. Another numerical scheme based on the linear complementarity formulation and the finite element method we used in [10].

For all the examples solved numerically we have used the data provided by Huo & Müller [7, 5]. After some calculations we obtain the following values: temperature $\theta = 292.6$ K, yielding stress $\sigma_Y = 64.227$ MPa, recovery stress $\sigma_R = 45.277$ MPa, elasticity modulus $E = 12\,300.0$ MPa, material constant $B = 1.30$ MPa, phase transition strain $\eta = 0.0686$, density of the alloy $\rho_{\text{dens}} = 7750.0$ kg/m^3, difference in energies $\Delta\psi^0 = \psi^0_{\mathcal{M}} - \psi^0_{\mathcal{A}} = 3.756$ J/m^3, $\gamma = 4.406$ MPa, $\mu = 843.78$ MPa. We have analyzed the test examples as the displacement-driven loading process of the bar of unit length, say $l_B = 1.00\,\mathrm{m}$. The following initial distribution of the volume fraction, $c(0,x) = 0$, and the discrete memory, $c_0(0,x) = 1$, are taken. The loading history is defined by the elongation function $\ell(t) = 0.07308t + 0.019538\sin(5.712t)$, which has a local maximum at $t = 0.40$ and a local minimum at $t = 0.70$: $\ell(0.4) = 0.044$ and $\ell(0.7) = 0.03639$. This loading program induces one internal loop, whereas the loading function used in Section 4.2 produces 3 internal loops, cf. Fig. 10b.

The purpose of the example considered in this section is to test both the material response and convergence properties of the suggested algorithm in the case of nonlinear inhomogenuity induced by the function $\alpha(x)$ and presence of body forces $f(t,x)$. We have calculated the bar with the variable cross-sectional area defined by the function $\alpha(x) = 0.90 + 0.10\cos(4\pi x/l_b)$, subjected to the elongation $\ell(t)$ applied at the bar's right end (the bar's left end being fixed) and the body force $f(t,x) = 20t(t-0.6)(t-1.1)\sin(8\pi x/l_B)$. Furthemore, the material is assumed to exhibit hardening with $L = 2B$.

The evolution of the volume fraction c with respect to time t is shown in Fig. 7a, whilst that of the associated discrete memory c_0 in Fig. 7b, both containing complement information on the hysteretic deformation process. Owing to the symmetry of the problem we display the distributions only for one half of the bar, i.e. $x \in [0, l_b/2]$. Since the figures are self-explanatory we merely note that during reloading the transformation process is first finished in the region where the internal loop like that in Fig. 1c is taking place. This is the situation at points $x \in (0.080, 0.118) \bigcup (0.382, 0.420)$ where the characteristic localization of volume fraction, or in other words of great straining can be observed, Fig. 7a. Such a localization of strain is due to the fact that the deformation process in a material point is actually stress-controlled, cf. also Fig. 6.

The results of the convergence test are gathered in Table 1. As a reference solution we have taken that for $\vartheta = \vartheta_{\mathrm{Ref}} = 0.04/512$ and $h = h_{\mathrm{Ref}} = 0.02/512$. The error is calculated as the averaged sum of differences in the force F at five selected times

$$e_i = \frac{1}{5}\sum_{k=1}^{5} |F_i(k\cdot 0.2) - F_{\mathrm{Ref}}(k\cdot 0.2)|$$

respectively, for different time steps ϑ while $h = h_{\mathrm{Ref}}$, and for different h while $\vartheta = \vartheta_{\mathrm{Ref}}$.

Table 1. Errors for various spacing h_i (with $\vartheta_{\mathrm{Ref}} = 0.04/512$) and time steps ϑ_i (with $h_{\mathrm{Ref}} = 0.02/512$).

h_i	e_i^h	ϑ_i	e_i^ϑ
$\bar{h}$=0.02	0.57468171	$\bar{\vartheta}$=0.04	0.00980176
$\bar{h}/2$	0.19339064	$\bar{\vartheta}/2$	0.00023222
$\bar{h}/4$	0.04137294	$\bar{\vartheta}/4$	0.00023222
$\bar{h}/8$	0.03295714	$\bar{\vartheta}/8$	0.00023222
$\bar{h}/16$	0.00237281	$\bar{\vartheta}/16$	0.00010923
$\bar{h}/32$	0.01563236	$\bar{\vartheta}/32$	0.00000514
$\bar{h}/64$	0.00673335	$\bar{\vartheta}/64$	0.00000514
$\bar{h}/128$	0.00224421	$\bar{\vartheta}/128$	0.00000004
h_{Ref}	0.0	ϑ_{Ref}	0.0

The obtained results show that in the considerd case the approximation in space is of decisive importance. As can be seen the algorithm exhibits a first order convergence in h. Further, being at first sight quite extraordinary, the results of convergence with respect to time step ϑ do reflect the intrisic property of the hysteresis operator that to calculate its output it sufficies to know just the collection of relative maxima and minima of the input functions. Note that in this example the input consists of the elongation $\ell(t)$ and the body force $f(t,x)$.

Figure 7: Distribution (a) of phase fraction c and (b) of discrete memory c_0 as a function of t and x.

4.2 Numerical study of internal loops

In this section we determine numerically the system behaviour of a inhomogeneous bar in the course of a number of loading/unloading cycles. The analysis here complemments the analytical results obtained in Sections 3.2 and 3.3. The bar possesses a linearly varying cross-sectional area $\alpha(x) = 0.9999 + 0.0002x$, $x \in (0, 0.5)$. Moreover, we take the same material parameters as in Section 4.1, except the hardening modulus L which we now express in terms of the parameter ρ, i.e. $L = 1.3 + 0.0002/\rho$. Our goal here is to test the influence of this measure of inhomogenuity on the system behaviour.

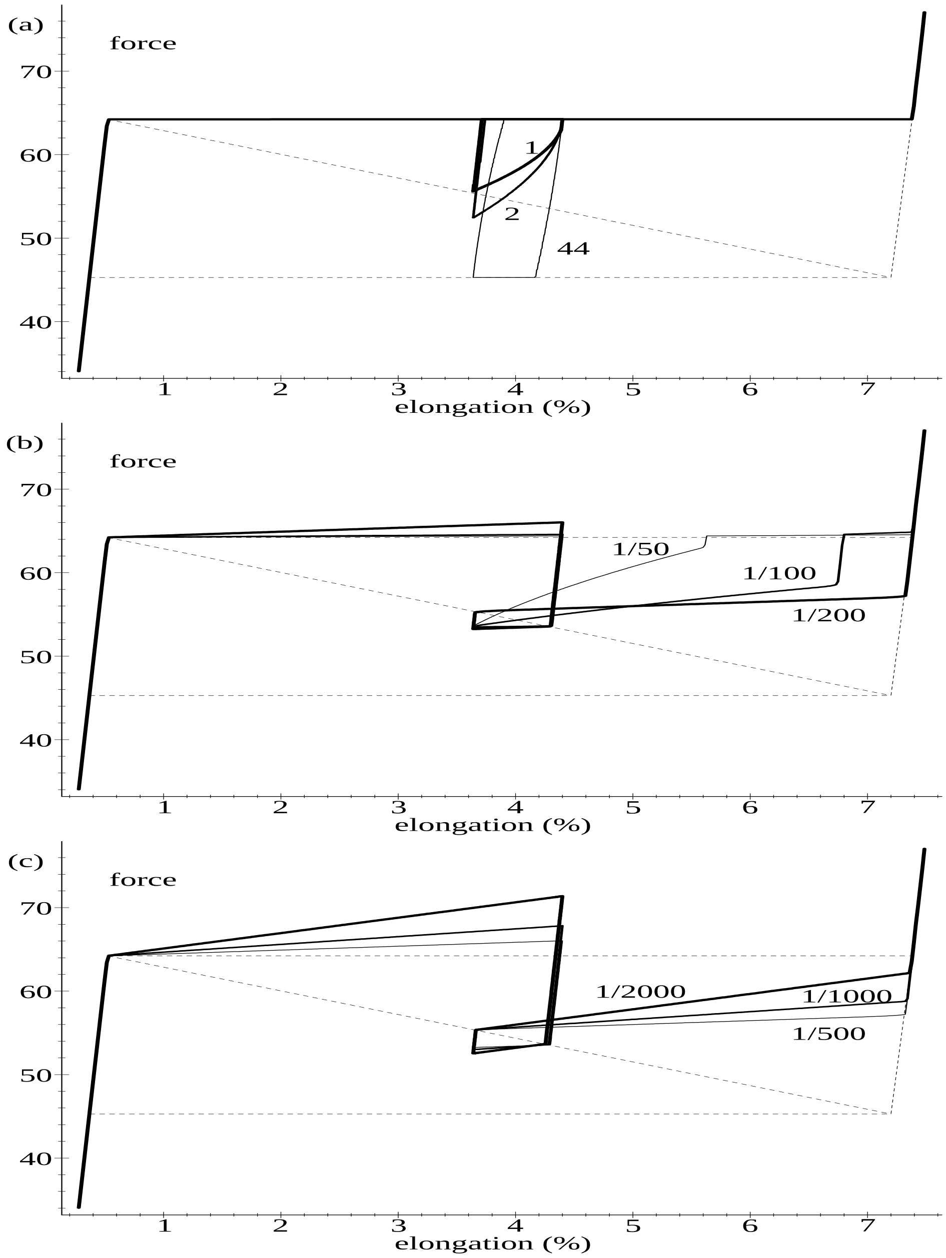

Figure 8: Nonhomogeneous case. Force F at the end of bar as a function of elongation ℓ of 7c, for various (scaled) inhomogeneuity parameter ρ/ρ_0.

First, we subject the bar to the loading program $\ell(t)$ shown in Fig. 7c. The induced system behaviour is displayed in Fig. 8 for some representative values of the inhomogenuity parameter ρ scaled against the characteristic value $\rho_0 = \alpha_0/(\gamma l_B)$. By a dotted line the diagonal and the recovery segment for the ideal pseudoelastic case $L = B = 1.30$ are marked. As established in Section 3.2, the internal loops are realized if the inhomogenuity of the process is sufficiently small, $\rho < \rho_0/200$, which results in uniform distributions of volume fraction c, see Fig. 9 for $\rho = \rho_0/500$. Otherwise we have in terms of strain a localization phenomenon. It should be stressed that the localization effect, even if not present after a first loading/unloading cycle, it may occur later in the course of the loading/unloading sequences.

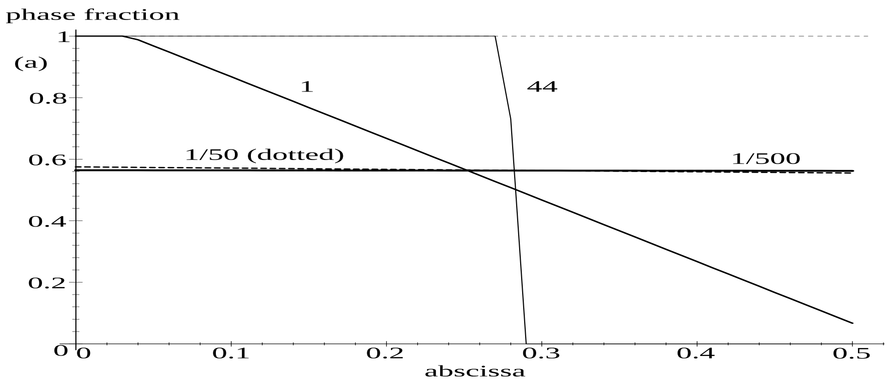

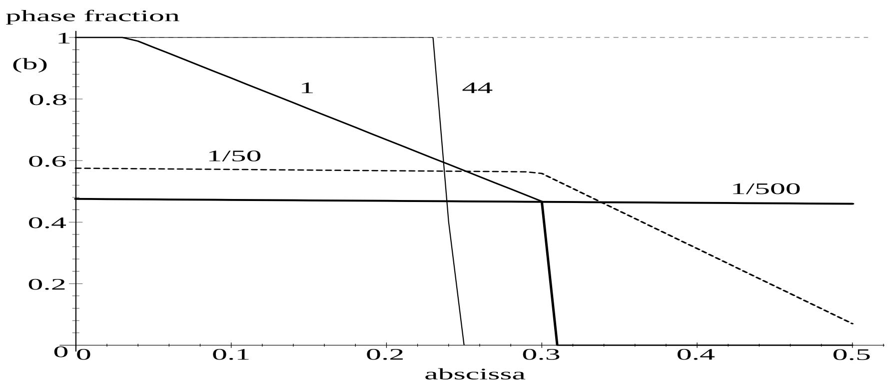

Figure 9: Nonhomogeneous case. Distribution of volume fraction $c(x)$ along the bar at the end of loading (a) and unloading (b), for various (scaled) inhomogenuity parameter ρ/ρ_0.

To further check the impact of some inhomogenuity induced by previous loading/unloading loops we have subjected the bar to the loading history shown in Fig. 10b. We denote by L1,L2,L3 and U1,U2,U3 the turning points of the sequential loading and unloading steps. The elongation program induces three internal loops with the same unloading amplitude of 0.6%. In Fig. 10 presented are the results which illustrate three types of the system behaviour. First, when the inhomogenuity is high (or hardening is small) there is no internal loop, in this example for $\rho = \rho_0/2 = 0.22694$. Then for $\rho = \rho_0/500$ even although the first loading/unloading cycle is accompanied by a regular hysteresis internal loop, the inhomogeneous state of strains which is induced by that cycle disturbs subsequently the regular response of the system, compare Figs. 10a and 8c. Notice the sharp knicks in Fig. 11a and b. Finally, some accumulation of the deformation history can also be observed in the case of the very small inhomogenuity $\rho = \rho_0/2000$ corresponding to the hardening modulus $L = 1.68B = 2.1813$, see Fig. 11c.

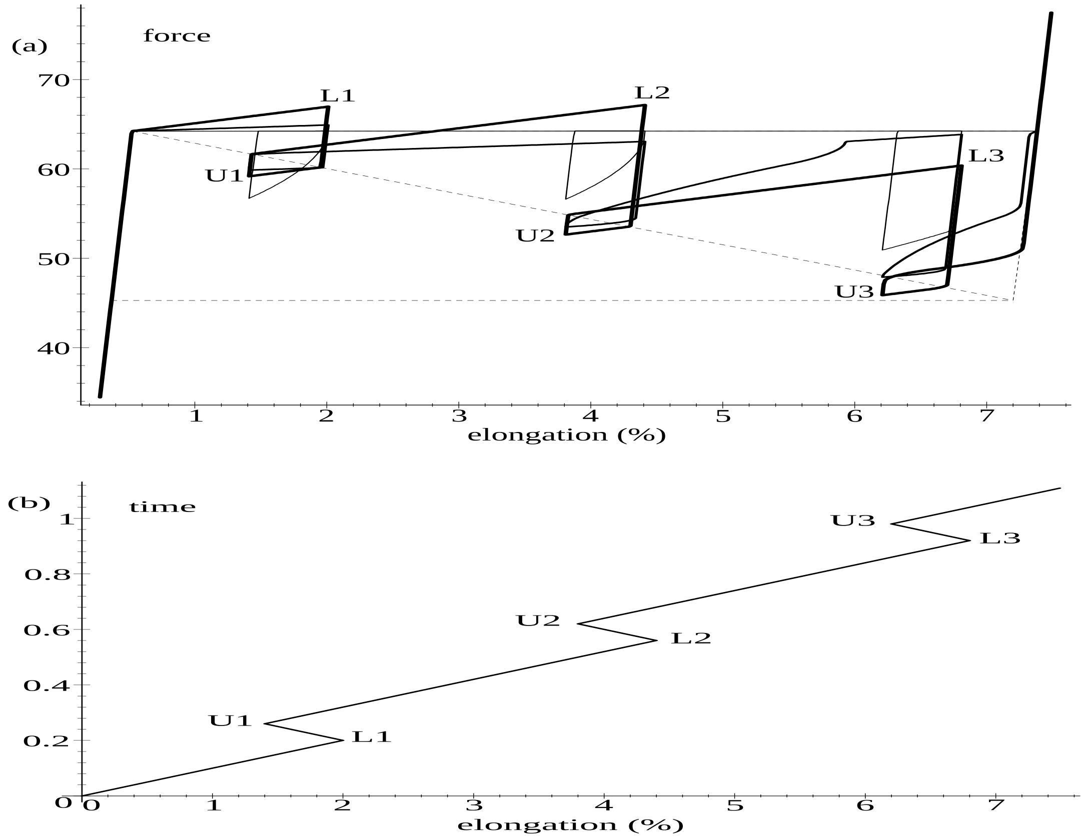

Figure 10: Nonhomogeneous case: (a) Force F at the end of bar as a function of elongation $\ell(t)$ shown in (b), for various (scaled) inhomogenuity parameter: $\rho/\rho_0 = 1/2$ (thin line), $\rho/\rho_0 = 1/500$ (medium line), $\rho/\rho_0 = 1/2000$ (thick line).

In closing this section we wish to briefly address the issue of parameter identification in the context of the considered model of pseudoelasticity. The model is defined by 5 parameters: $E, \eta, B, L, \Delta\psi^0$ which can easily be determined from the stress-strain (force-elongation) diagram. To show this we refer to Fig. 1 and denote the coordinates of the characteristic points as follows A$(\varepsilon_Y^0, \sigma_Y^0)$, B$(\varepsilon_Y^1, \sigma_Y^1)$, D$(\varepsilon_R^1, \sigma_R^1)$, E$(\varepsilon_R^0, \sigma_R^0)$. (Note that due to the symmetry of the model 3 coordinates are redundant.) From the relations defining the model we arrive at the system of equations

$$E\varepsilon_Y^0 = \sigma_Y^0, \quad \eta = \varepsilon_Y^1 - \varepsilon_Y^0, \quad B/\eta = \sigma_Y^0 - \sigma_R^1, \quad (\Delta\psi^0 + B/2)/\eta = \sigma_Y^0, \quad (L-B)/\eta = \sigma_Y^1 - \sigma_Y^0,$$

the solution of which allows us to express the model's parameters in terms of the experimentally measured quantities:

$$E = \sigma_Y^0/\varepsilon_Y^0, \quad \eta = \varepsilon_Y^1 - \varepsilon_Y^0, \quad B = (\sigma_Y^0 - \sigma_R^1)(\varepsilon_Y^1 - \varepsilon_Y^0),$$

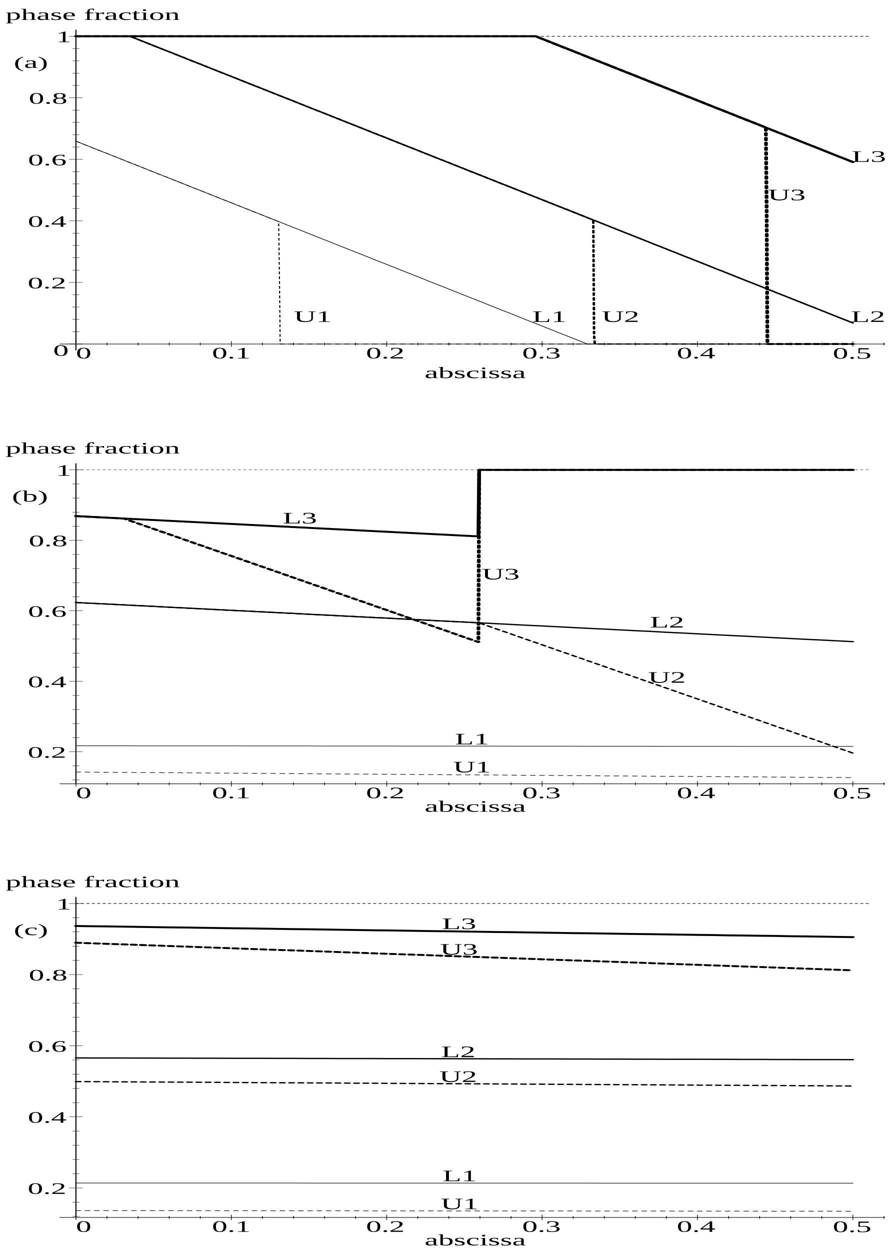

Figure 11: Nonhomogeneous case. Distribution of volume fraction $c(x)$ along the bar at the end of the loading and unloading steps shown in Fig. 10b, for (a) $\rho/\rho_0 = 1$, (b) $\rho/\rho_0 = 1/500$, (c) $\rho/\rho_0 = 1/2000$.

$$L = (\sigma_Y^1 - \sigma_R^1)(\varepsilon_Y^1 - \varepsilon_Y^0), \quad \Delta\psi^0 = \frac{1}{2}(\sigma_Y^0 + \sigma_R^1)(\varepsilon_Y^1 - \varepsilon_Y^0).$$

Now, with reference to the experimental tests of Müller *et al.* [7, 5] (wire of diameter $d = 0.0024$ m and $l_B = 0.034$ m) if we assume "nearly ideal" pseudoelasticity by letting $\omega = (\sigma_Y^1 - \sigma_Y^0)\eta$ be equal to 0.1η and $\rho\omega = 10^{-9}$, then for $\eta = 0.0686$ we obtain that the inhomogenuity parameter $\rho \approx \rho_0/200$. In light of our numerical experiments such inhomogenuity will be high enough to impede development of regular internal loops on the level of system behaviour, in case of more than one loading/unloading cycles, cf. Figs. 8b and 10a.

5 Conclusions

We have developed a mathematical formulation and a numerical scheme for the 1D pseudoelastic phase transformation process. The numerical algorithm is based on the idea of monotone path rule in which the deformation process is decomposed into a sequence of piecewise monotone responses. The thermomechanical model studied allows one to account for hysteresis effects including those induced by internal loops. It turns out that the local material behaviour is different from that observed at the level of global quantities describing the deformation process. Due to the high complexity of the hysteretic response the model's predictions are very sensitive to any inhomogenuity in the two-phase system. Even if the material of a body exhibits remarkable hardening a sequence of loading/unloading steps can produce in the body a number of localized strain regions. However, the loss of material stability for the material model used is of special kind because local deformamation is eventually arrested when the (direct or reverse) phase transformation is finished and the material stiffness is recovered. Although the results are obtained for one dimensional test problems they reveal the kind of difficulties one will be faced with to a greater extent when dealing with the corresponding two or three dimensional problems.

References

[1] J.M. BALL, C. CHU, and R.D. JAMES. Hysteresis during stress-induced variant rearrangement. *J. de Physique IV, Coll. C8, suppl. J. de Physique III*, 5:C8–245–C8–251, 1995.

[2] M. BROKATE and J. THEEL. Some numerical simulations of pseudoelastic hysteresis shape memory alloys. *Continuum Mech. Thermodyn.*, 5:265–280, 1993.

[3] B. FEDELICH and G. ZANZOTTO. One-dimensional quasistatic nonisothermal evolution of shape-memory material inside the hysteresis loop. *Continuum Mech. Thermodyn.*, 3:251–276, 1991.

[4] M. FREMOND. *Shape memory alloy. A thermomechanical macroscopic study*, volume 351 of *CISM*, chapter 1, pages 1–67. Springer, Wien, New York, 1996.

[5] S. FU, Y. HUO, and I. MÜLLER. Thermodynamics of pseudoelasticity - an analytical approach. *Acta mechanica*, 99:1–19, 1993.

[6] E. HORNBOGEN. On the term 'Pseudo-elasticity'. *Z. Metallkd.*, 86(5):341–344, 1995.

[7] Y. HUO and I. MÜLLER. Nonequlibrium thermodynamics of pseudoelasticity. *Continuum Mech. and Thermodyn.*, 5:163–204, 1993.

[8] R.V. KOHN. The relaxation of a double-well energy. *Continuum Mech. Thermodyn.*, 3:193–236, 1991.

[9] M.S. KUCZMA, V.I. LEVITAS, A. MIELKE, and E. STEIN. Nonisothermal hysteresis loops in pseudoelasticity. In Proceedings of the XIII Conference on *Computer Methods in Mechanics*, pages 711–718, Poznan, 5-8 May 1997.

[10] M.S. KUCZMA and A. MIELKE. Variational approach to pseudoelastic behaviour. *ZAMM*, 77, Suppl. 1,:S175–S176, 1997.

[11] A.V. LEVITAS, V. I. IDESMAN and E. STEIN. Finite element simulation of martensitic phase transformations in elastoplastic materials. *Int. J. Solids Structures*, 35:855–887, 1998.

[12] V. I. LEVITAS. Thermomechanical description of pseudoelasticity — the threshold-type dissipative force with discrete memory. *Mech. Res. Comm.*, 21:273–280, 1994.

[13] V.I. LEVITAS. *Thermomechanics of Phase Transitions and Inelastic Deformations of Microinhomogeneous Materials* (in Russian). Naukova Dumka, Kiev, 1992.

[14] I. MÜLLER and S. SEELECKE. Thermodynamic aspects of shape memory. Trans Tech Publications (submitted), 1996.

[15] B. RANIECKI, CH. LEXCELLENT, and K. TANAKA. Thermodynamic models of pseudoelastic behaviour of shape memory alloys. *Arch. Mech.*, 44(3):261–284, 1992.

[16] R.C. ROGERS. Some remarks on nonlocal interactions and hysteresis in phase transitions. *Continuum Mech. Thermodyn.*, 8:65–73, 1996.

[17] J.A. SHAW and S. KIRIAKIDES. Thermomechanical aspects of NiTi. *J. Mech. Phys. Solids*, 43(8):1243–1281, 1995.

[18] K. WILMANSKI. On pattern formation in stress-induced martensitic transformation. In G. Maugin and W. Muschik, editors, *Nonlinear Thermodynamical Processes in Continua*, pages 88–105, Berlin, 1992. TU Berlin.

[19] K. WILMANSKI. Model of stress-strain hysteresis loops in shape memory alloys. *Int. J. Engng Sci.*, 31(8):1121–1138, 1993.